ARCHIVES OF ELECTRICAL ENGINEERING VOL. 66(4), pp. 829-842 (2017)

DOI 10.1515/aee-2017-0063

# Frequency and time domain characteristics of digital control of electric vehicle in-wheel drives

**LESZEK JARZEBOWICZ, ARTUR OPALINSKI**

*Faculty of Electrical and Control Engineering, Gdansk University of Technology*
*Narutowicza St. 11/12, 80-233 Gdansk, Poland*
*e-mail: leszek.jarzebowicz@pg.edu.pl, aopalin@gmail.com*

(Received: 28.09.2016, revised: 30.07.2017)

**Abstract:** In-wheel electric drives are promising as actuators in active safety systems of electric and hybrid vehicles. This new function requires dedicated control algorithms, making it essential to deliver models that reflect better the wheel-torque control dynamics of electric drives. The timing of digital control events, whose importance is stressed in current research, still lacks an analytical description allowing for modeling its influence on control system dynamics. In this paper, authors investigate and compare approaches to the analog and discrete analytical modeling of torque control loop in digitally controlled electric drive. Five different analytical models of stator current torque component control are compared to judge their accuracy in representing drive control dynamics related to the timing of digital control events. The Bode characteristics and step-response characteristics of the analytical models are then compared with those of a reference model for three commonly used cases of motor discrete control schemes. Finally, the applicability of the presented models is discussed.

**Key words:** variable speed drives, modeling, digital control events, anti-lock braking, in-wheel drives

## 1. Introduction

Application of in-wheel electric drives brings new capabilities to electric and hybrid vehicles. These drives are promising for the role of actuators in active safety systems [1] such as the anti-lock braking system (ABS) and electronic stability program (ESP), as they enable controlling torque separately for each wheel. The control dynamics are much better with electric drives than with traditional, hydraulic brakes. Hence, in-wheel drives may substantially improve the efficiency of the safety systems.

Electric or blended hydraulic-electric ABS and ESP systems require dedicated control algorithms. Although they have attracted the attention of researchers [2, 3], their validation and verification is predominantly based on simulation in the time domain. A review [4] of current research on traction control and the ABS in electric vehicles summarizes that 65% of papers rely on computer simulations in the time domain to verify the proposed safety algo-

rithms. In simulation models, the torque reference signal is set by a safety control algorithm separately for each electric drive and it is usually assumed to be applied to the wheels without delay [4]. The mechanics of wheels and of vehicles are researched [3, 6], without considering details of electric drive phenomena. In other work [7], a detailed model of an induction motor used as an ABS actuator has been built; however, the controller is described and simulated in continuous time.

Suggestions for the safety systems' control bandwidth can be concluded from the paper by M'sirdi et al. [8], which describes an observer for estimation of vehicle dynamical parameters based on the angular wheel speed sensors of a standard hydraulic ABS. The vehicle state observer exploits a sampling frequency in the range of approximately 130 Hz to 461 Hz for a vehicle speed range between 50 km/h and 164 km/h. The dynamic characteristics of electromechanical actuators in the ABS have also been analyzed in a range up to about 12 Hz [9]. In contrast, the torque bandwidth of vehicle in-wheel electric motor drives is assumed to be up to approximately 10 Hz for ASR control and less than 200 Hz for an ABS [10]. This research stresses the significance of modeling control dynamics over a specific frequency range and provides the requirements for the torque control bandwidth for electric drive. The dynamic properties of a blended hydraulic-electric ABS have further been investigated by Savitski et al. [11]. It was experimentally confirmed by road tests that the operating frequency of blended braking systems reaches 10 Hz, while a typical hydraulic ABS operates in the range of 1 Hz - 3 Hz. Consequently, substantial differences in braking distance as well as in driving comfort can be noticed between classical and blended anti-lock braking systems.

The impact of techniques of current sampling in a mixed analog-discrete control system has been investigated by Opalinski and Jarzebowicz [12] solely in the frequency domain, indicating no significant differences in the range of frequencies currently emerging in an ASR and ABS. On the other hand, the torque control bandwidth in digitally controlled systems is ultimately limited by the output update rate of the control algorithm [13]. Replacing an analog control with a sampled one negatively influences the electric drive control dynamics [14] if the control cycle, which also influences the power electronic converter switching frequency, is not radically shortened. Moreover, the exact instant of motor currents sampling within the control period influences the control characteristics significantly, as researched for both PMSM and DC drives [15, 16].

## 2. Problem formulation

Existing research on safety algorithms for electric vehicles ignores the issues of modeling digitally controlled electric drives. The timing of digital control events, whose importance has been recalled in the previous section, still lacks an analytical description for modeling its influence on control system dynamics. Therefore, new models of an electric drive are urgently needed to evaluate vehicles' stability and anti-lock braking systems by simulations.

Obviously, not only motor parameters, but also a drive control algorithm with its digital implementation details influence the motor torque control dynamics. The timing of digital

control events may be precisely represented in hybrid continuous-discrete models. These models, however, do not provide the complete analytical description needed for more comprehensive analysis and easier implementation of vehicle traction control systems.

Contrasting the findings originating from control system characteristics in the frequency domain with the characteristics of the time domain is essential to give a complete picture of the control system behavior, and to pinpoint application-specific tradeoffs between control quality indicators from these two domains. Such discrete-time modeling is important for drive controller design when specific dynamic characteristics are imposed, according to Hinkkanen et al. [17].

Therefore, this paper compares five different analytical models to judge their accuracy in representing the drive control dynamics related to the timing of digital control events. Three cases of motor current sampling are considered. The Bode characteristics and step-response characteristics of these models and of an exemplary real PMSM drive are compared, using a precise hybrid model of the drive as a reference. The reference model, which has been validated in previous work, includes continuous-time motor equations an the digital implementation of the control algorithm.

## 3. Digital control of electric drive

Torque control in an electric motor is closely related to motor current control, because motor torque depends on a motor current. Thus, the current control loop in an electric drive, as depicted in Fig. 1, constitutes a torque control loop as well. A digitally imlemented PI controller is usually used to drive motor torque [13, 15].

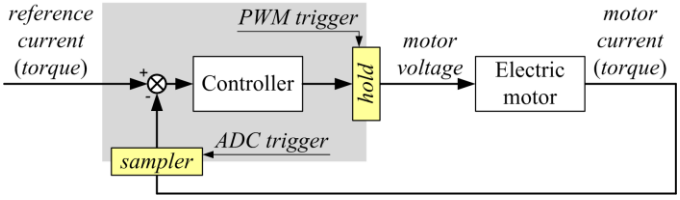


Fig. 1. General representation of the torque control loop in electric drive

While an electric motor can be represented well in continuous time, the control algorithm cannot, because it is performed digitally as a series of discrete control events. The transistors in a power electronic converter that supplies the motor, have a limited switching frequency. Therefore, the frequency of pulse width modulation $f_{\mathrm{PWM}}$, closely related to the reference voltage update rate, is typically in the range from 2 kHz to 20 kHz. Hence, the control algorithm runs once in every control cycle $T[k]$, and the resulting reference voltage is held constant over the whole $T[k+1]$ cycle. The frequency of control cycles is related to the update rate of the reference voltage, which is a digital control event that influences the dynamic properties of the control system.

In addition, the sampling instant of the motor current within the control cycle constitutes another digital control event. Its timing should be considered in controller modeling, as it influences the controller feedback signal. Sampling must precede the update of the resulting voltage by a time range long enough to accomplish all control algorithm computations. Sampling is typically performed at the beginning or in the middle of the control cycle in AC drives with symmetric PWM, as marked with squares on the time axis in Fig. 2 for $m = 0$ or for $m = T/2$. Such sampling introduces one-cycle ($T$) delay or half-cycle ($T/2$) delay, respectively, between sampling the current and updating the output voltage. A less common approach is to sample the current both at the beginning and in the middle of the control cycle, and to use these samples for estimating the zero-delay current value, as shown in Fig. 2 for $m = T$.

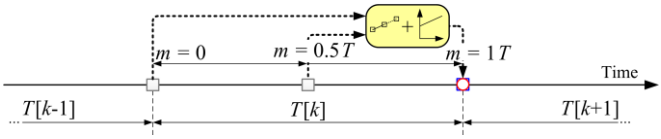


Fig. 2. Timing of digital events in current control cycles for sampling at the beginning of the control cycle ($m = 0$), sampling in the middle of the control cycle ($m = T/2$), and estimating the zero-delay current value ($m = T$)

## 4. Transfer function approaches to modeling digital control events in electric drive

Digitally controlled electric drives feature repeating instants of feedback sampling and output update. These instants are not considered in typical continuous models using $s$-domain, where both feedback measurement and output update are assumed to take place continuously. Discrete models in $z$-domain encompass consecutive, evenly spaced instants; however, in typical approaches, these instants represent both sampling and output update, which occur simultaneously. This is over-simplistic when researching non-simultaneous events in electric drives. Transfer functions described in this section represent different approaches to include the digital control events in either the $s$- or the $z$-domain.

The duration of control cycle $T$ must follow the Shannon-Nyquist theorem and is usually selected to satisfy $T \ll \tau$, where $\tau$ is the electrical time constant of the motor. This enables modeling the system in the continuous-time domain. If, additionally, reference signal $r(t)$ and motor current $i(t)$ are sampled at the same instant of time, then the output signal $u[k + 1]$ of the digital controller is given as

$$u[k+1] = f\left(r\left((k+m)\cdot T\right) - i\left((k+m)\cdot T\right)\right), \tag{1}$$

where the right-hand side of the equation describes a control law.

The electric motor as a first-order inertia is described by $P(s)$ and the PI controller by $C(s)$:

$$P(s) = K/(1+\tau s),\ C(s) = K_p(1+K_i/s). \tag{2}$$

To model the impact of parameter $m$ in (1) on the dynamic properties of the control system, different extensions of the basic transfer function models are described below. The forthcoming discussion uses (2) to represent the motor and controller, but the general approach to modeling digital control events in electric drives is not limited to this type of plant or controller.

The considered models, which differently represent the details of the digital control of electric drives, are presented in Fig. 3 and described in the following subsections (4.1-4.5). The three continuous-time (analog) models, depicted in Fig. 3a, differ in regard to including or neglecting the delay blocks *ID* and *OD*. The models use reference signal $r(t)$, error signal $e(t)$, control signal $u(t)$, and the controlled motor current $i(t)$. The two digital models have a common structure, as shown in Fig. 3b, but they differ with respect to the mathematical description of the plant. The digital models use reference signal $r[k]$ and error signal $e[k]$, defined for discrete time instants $k \cdot T$, where $k = 1, 2, 3,\ldots$

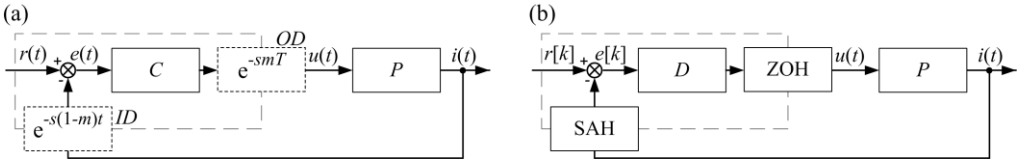


Fig. 3. Control system models structure: a) analog models optionally using delay blocks *ID* and *OD;* b) digital models using two diffrerent plant *P* models

### 4.1. Analog model *A*1

This is the basic model formulated in the *s*-domain and consists only of the plant and the controller transfer functions (Fig. 3a, without blocks *ID* and *OD*). Such a modeling approach does not include any digital control events, and its closed-loop transfer function is

$$G(s) = \frac{C(s)\cdot P(s)}{1 + C(s)\cdot P(s)} = \frac{KK_p s + KK_i K_p}{\tau s^2 + (1 + KK_p)s + KK_i K_p}. \tag{3}$$

As parameter $m$ is not included in (3), the sampling delay during verification may be reflected only indirectly by selecting the controller gain $K_p$ suitable for a particular sampling variant.

### 4.2. Analog model *A*2

The update of the controller output at instant $(k + 1)\cdot T$ is computed based on the feedback signal sample from $k \cdot T + m$, as depicted in Fig. 2. Thus, there is a delay of $(1 - m)\cdot T$ between the considered instants. This delay in the *A*2 model is represented by the *ID* transportation delay (i.e. dead-time) of $(1 - m)\cdot T$, placed in the feedback loop, as shown in Fig. 3a. The closed-loop transfer function of *A*2 is

$$G(s) = \frac{C(s)\cdot P(s)}{1 + e^{-s(1-m)T}\cdot C(s)\cdot P(s)} = \frac{KK_p s + KK_i K_p}{\tau s^2 + (1 + KK_p e^{-s(1-m)T})\cdot s + KK_i K_p e^{-s(1-m)T}}. \tag{4}$$

Supplementing (3) with the delay creates non-polynomial transfer function (4). This, in turn, makes the analytical determination of dynamic properties troublesome. Hence, to return to the polynomial form of (4), the exponent $e^{-s\,(1-m)\,T}$ is approximated by using the Padé formula. While the Padé approximation does not introduce unstable poles in the case of the same order in the nominator and denominator [17], it may change the Bode characteristics and also cause the control loop to become unstable [19]. A time delay is featured by a unity gain at all frequencies, with the phase lag being a linear function of the frequency. Although the Padé approximation reflects the gain correctly, the phase lag characteristics may diverge from the original ones, especially at high frequencies. Increasing the order of approximation improves accuracy, but only for a limited frequency range [20]. Moreover, high-order approximations result in clustered poles of transfer functions, which increase sensitivity to perturbations [21]. However, as long as assumption $T \ll \tau$ holds, the time constant of the dominant lag in the system is much greater than the dead-time. Consequently, the Padé approximation can be used during outer closed-loop stability analysis for approximately the first 180°-360° of the phase lag without the need for memory shift-registers and interpolation techniques.

### 4.3. Analog model *A*3

While the *A*2 model includes the impact of *m* on the system properties, it does not express the limited controller output rate corresponding to its digital implementation. To represent the real system more precisely, the *A*3 model is supplemented with the additional *OD* delay in the forward path. In the modeled system, the controller output changes at instants $k \cdot T$ and it is held until $(k + 1) \cdot T$. The resulting delay progresses from zero to *T*. Thus, the delay may be simply averaged to *T*/2 in the *s*-domain, adding to the delay of $(1 - m) \cdot T$ caused by selected sampling timing.

Another approach considers the range of delay variation for the accumulated effects of sampling and the output rate. For $m = 1$ and an output updated at the beginning of the control cycle, the total delay of the control system is zero. In turn, for $m = 0$ and an output update at the end of the control cycle, the total delay reaches 2*T*. This translates into an average total delay of *T*. Following the second approach, the feedback path delay is set to $(1 - m) \cdot T$, and the controller output update is delayed by a further $m \cdot T$ (Fig. 3a, with delay blocks *ID* and *OD*). These delays result in a total control loop delay of *T*. The closed-loop transfer function for *A*3 is then

$$G(s)=\frac{e^{-smT}\cdot C(s)\cdot P(s)}{1+e^{-smT}\cdot e^{-s(1-m)T}\cdot C(s)\cdot P(s)}=\frac{e^{-smT}\cdot C(s)\cdot P(s)}{1+e^{-sT}\cdot C(s)\cdot P(s)}=\frac{\left(KK_ps+KK_iK_p\right)e^{-smT}}{\tau s^2+\left(1+KK_pe^{-sT}\right)\cdot s+KK_iK_pe^{-sT}}. \quad (5)$$

This model includes the average total control system delay in term $e^{-sT}$. Thus, *A*3 represents the sampling by parameter *m* as well as control period duration by parameter *T*. Similar to *A*2, the Padé approximation is also applicable here to enable analytical analysis of model's dynamic properties.

### 4.4. Digital model *D*1

Analog models *A*1, *A*2 and *A*3 are based on continuous functions that do not represent digital control events directly. Digital modeling in the *z*-domain reflects differently the digital

features of the controller. It assumes that the feedback signal is available only at sampling instants. This is represented in Fig. 3b by an analog-to-digital converter, which performs sample-and-hold (SAH). Indeed, the presence of SAH does not result in any additional terms in the transfer function of the system. As for the controller's output update, the signal is passed to the plant through a digital-to-analog converter performing the zero-order-hold (ZOH) operation. This represents the cyclical update of the PWM control registers in the digital controller. ZOH can be modeled in the *s*-domain by $\mathrm{ZOH}(s)(1 - e^{sT})/s$.

The *z*-domain transfer function of the controller *C* can be derived from (2) by using, for example, the Euler forward method. The *s*-domain function of the plant *P* is first combined with the ZOH(*s*) and then converted into the *z*-domain by pole and zero matching. Finally, the control system closed-loop transfer function for the *D*1 model is given by

$$G(z) = \frac{D(z)\cdot P_{\mathrm{ZOH}}(z)}{1 + D(z)\cdot P_{\mathrm{ZOH}}(z)} = \frac{A\cdot z + B}{C\cdot z^2 + D\cdot z + E}, \tag{6}$$

where:

$$A = KK_p\left(1 - e^{-T/\tau}\right), \quad B = K\left(K_pK_iT - K_p\right)\left(1 - e^{-T/\tau}\right), \quad C = 1,$$
$$D = K_pK - K_pKe^{-T/\tau} - 1 - e^{-T/\tau}, \quad E = K\left(K_pK_iT - K_p\right)\left(1 - e^{-T/\tau}\right).$$

The *D*1 model includes the discrete update of the controller's output signal; however, it does not reflect all the possible sampling variants since the sampling and update are assumed to happen simultaneously at instants $k \cdot T$. Thus, *D*1 can precisely model the sampling variants of $m = 0$ or $m = 1$. Sampling within the control cycle *T* cannot be included in the pure *z*-domain transfer functions.

### 4.5. Digital model *D*2

Instants occurring within a control cycle *T* can be modeled by using the modified *Z* transform [22]. In such a case, the control period boundaries have to be shifted so that the period *T* starts at the instant of the feedback signal sampling. Consequently, ZOH is modeled by a delay of $(1 - m) \cdot T$. By associating this delay with the plant's transfer function, and using the obtained polynomial, the closed-loop control system transfer function for *D*2 is

$$G(z) = \frac{D(z)\cdot P_m(z)}{1 + D(z)\cdot P_m(z)} = \frac{A\cdot z^2 + B\cdot z + C}{D\cdot z^3 + E\cdot z^2 + F\cdot z + C}, \tag{7}$$

where:

$$A = KK_p\left(1 - e^{-mT/\tau}\right), \quad B = KK_p\left(e^{-mT/\tau} - e^{-T/\tau}\right) + \left(1 - e^{-mT/\tau}\right)\left(K_iT - 1\right),$$
$$C = KK_p\left(K_iT - 1\right)\left(e^{-mT/\tau} - e^{-T/\tau}\right), \; D = 1, \; E = KK_p\left(1 - e^{-mT/\tau}\right) - e^{-mT/\tau} - 1, \; F = e^{-T/\tau} + B.$$

## 5. Comparison of the models

The transfer functions described in the previous section were compared with a hybrid reference model of a PMSM drive (Fig. 4, Table 1), whose technical parameters are provided in [15]. The model comprises a continuous model of an electric motor and a discrete controller model describing field-oriented control, which is usual in drive control research [23, 24]. The reference model has been thoroughly verified and validated by Jarzebowicz [15, 25], indicating a very good representation of real digitally controlled drive behavior.

Table 1. Transfer functions' constants

| Constant | Value |
|---|---|
| Digital controller sampling period $T$ | $10^{-4}$ |
| Plant time constant $\tau$ | 0.00875 |
| Plant gain $K$ | 8.3(3) |
| Controller proportional gain $K_p$ | 3.64 for $m = 0$, or 5.18 for $m = 0.5$, or 11.06 for $m = 1$ |
| Controller integral gain $K_i$ | 114.29 |

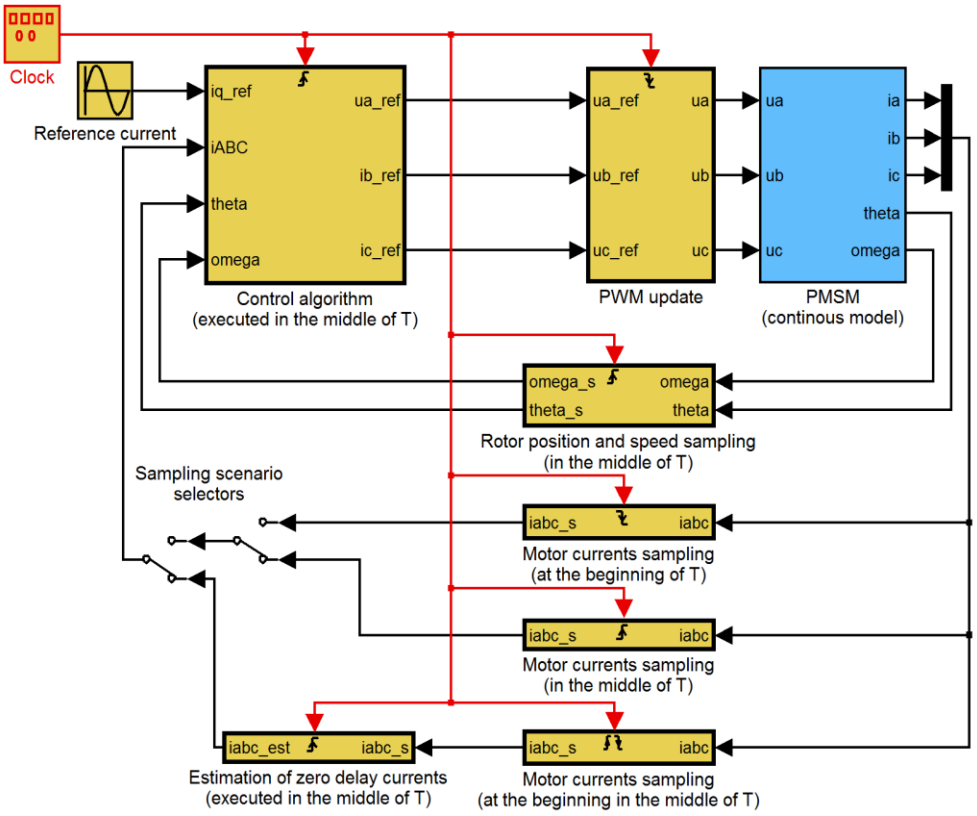


Fig. 4. Reference model of the PMSM drive implemented in Simulink

The comparison covers three variants of sampling delay parametrized by $m$ (i.e. $m = 0$, $m = 0.5$ and $m = 1$). The sampling delay substantially influence the dynamic properties of the control system, so the controller gain $K_p$ was selected individually for each variant. As in vehicle drives a small current overshoot is allowed to shorten the rise time [26], the authors tuned the gain $K_p$ in the reference model to obtain a 5% overshoot in response to a reference torque step change. The differences in controller gain $K_p$ reflect the differences between the different $m$ variants, even in the case of models that do not include parameter $m$.

The models were analyzed in terms of their step-command response and Bode plots. The graphs are given in Figs. 5-7. The main parameters of the step responses are summarized in Table 2. For research on time-based characteristics, a step from 0 to 1 p.u. is applied to the reference torque at $t = 0$. The time range on the step-response graphs is limited to 1 ms, which is sufficient to obtain a settled response in the reference model. The settling time is measured by assuming a 2%-wide band around 1 p.u. The rise time is measured for an output change from 0% to 90% of 1 p.u. As all derived Bode plots are flat for low frequencies, the graphs start from 100 Hz. The upper frequency limit of 5 kHz corresponds to the Nyquist frequency for discrete systems with a control rate of 10 kHz. The distinctive parameters related to the Bode plots are summarized in Table 3. The numbers in brackets represent relative errors with respect to the reference output.

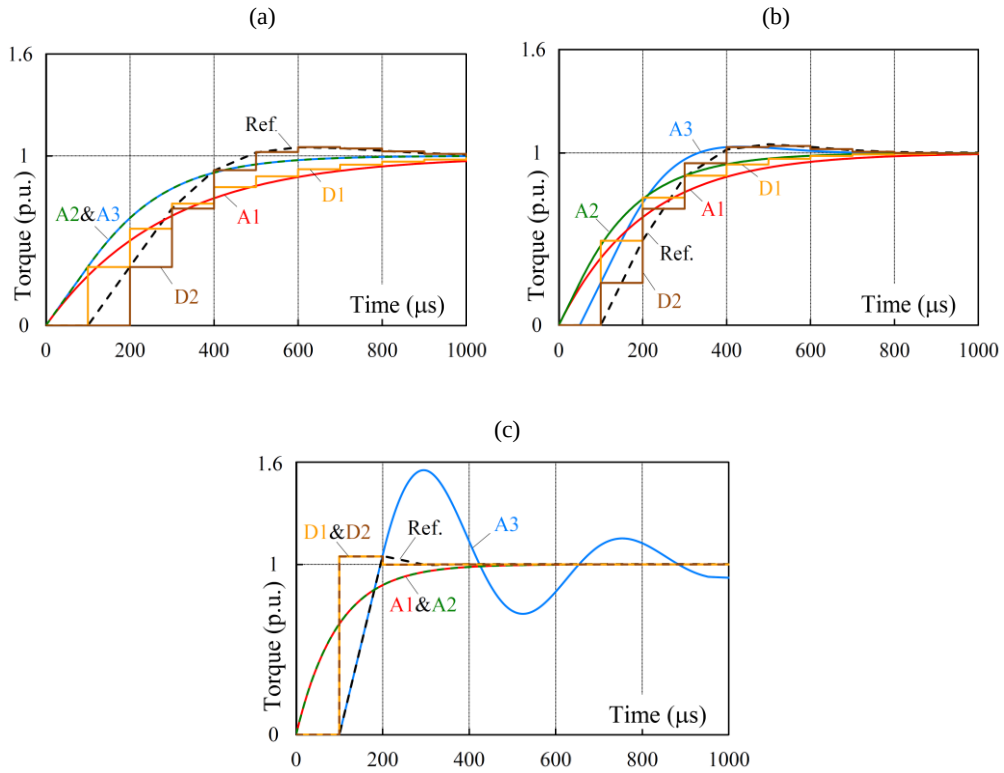


Fig. 5. Step-response graphs for: (a) $m = 0$; (b) $m = 0.5$; (c) $m = 1$

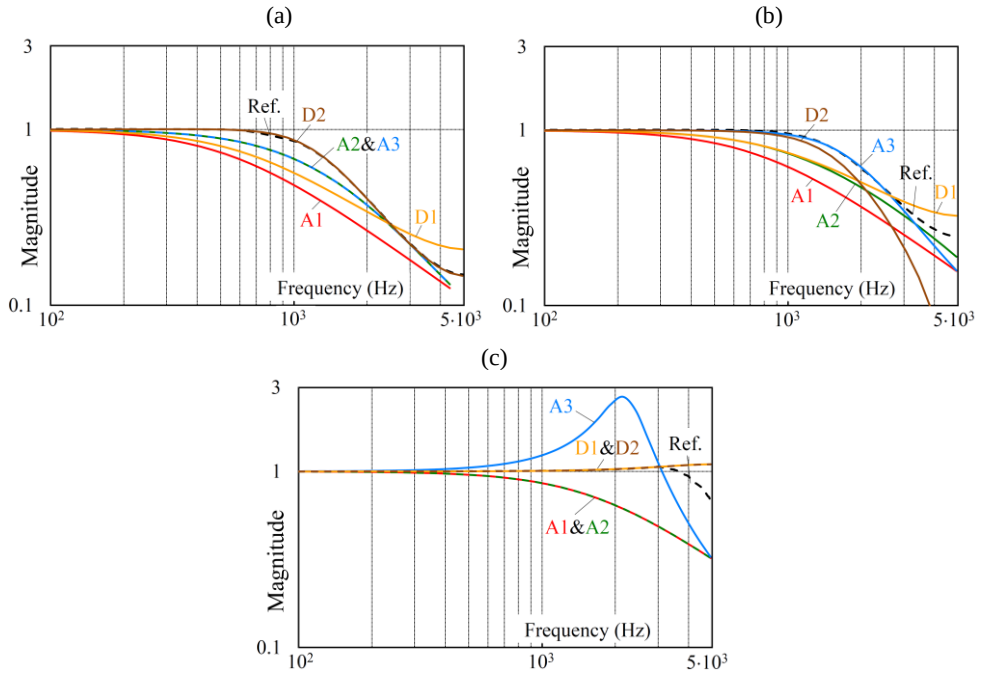


Fig. 6. Bode magnitude plots for: (a) $m = 0$; (b) $m = 0.5$; (c) $m = 1$

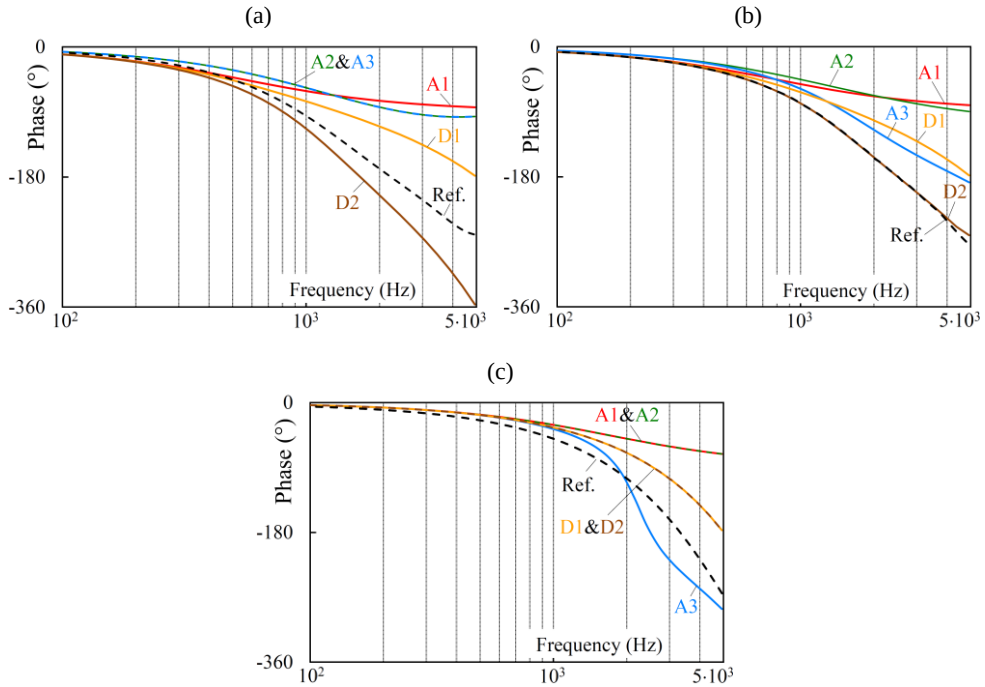


Fig. 7. Bode phase plots for: (a) $m = 0$; (b) $m = 0.5$; (c) $m = 1$

Table 2. Summary of the step responses

| Model | Rise time ($\mu$s) | | | Overshoot (%) | | | Settling time ($\mu$s) | | |
|---|---|---|---|---|---|---|---|---|---|
| | ***m* = 0** | ***m* = 0.5** | ***m* = 1** | ***m* = 0** | ***m* = 0.5** | ***m* = 1** | ***m* = 0** | ***m* = 0.5** | ***m* = 1** |
| Ref. | 394 | 324 | 186 | 5.00 | 5.00 | 5.00 | 873 | 678 | 256 |
| *A*1 | 664 (69%) | 467 (44%) | 218 (17%) | 0.00 (100%) | 0.00 (100%) | 0.00 (100%) | >1 ms (>15%) | 793 (17%) | 371 (45%) |
| *A*2 | 399 (1%) | 340 (5%) | 219 (18%) | 0.00 (100%) | 0.00 (100%) | 0.01 (100%) | 634 (27%) | 571 (16%) | 372 (45%) |
| *A*3 | 399 (1%) | 261 (19%) | 179 (4%) | 0.00 (100%) | 3.63 (27%) | 55.3 (1100%) | 634 (27%) | 553 (18%) | >1 ms (>300%) |
| *D*1 | 600 (52%) | 500 (54%) | 100 (46%) | 0.00 (100%) | 0.00 (100%) | 4.73 (5%) | 1000 (15%) | 600 (12%) | 200 (22%) |
| *D*2 | 400 (2%) | 400 (23%) | 100 (46%) | 5.17 (3%) | 4.05 (19%) | 4.72 (6%) | 900 (3%) | 700 (3%) | 200 (22%) |

Table 3. Summary of the Bode magnitude and phase plots

| Model | Corner frequency (Hz) | | | Phase drop (deg) at 5 kHz | | |
|---|---|---|---|---|---|---|
| | ***m* = 0** | ***m* = 0.5** | ***m* = 1** | ***m* = 0** | ***m* = 0.5** | ***m* = 1** |
| Ref. | 1040 | 1800 | 4700 | 260 | 270 | 250 |
| *A*1 | 550 (47%) | 800 (56%) | 1400 (70%) | 84 (68%) | 81 (70%) | 71 (72%) |
| *A*2 | 950 (9%) | 1050 (42%) | 1400 (70%) | 96 (63%) | 89 (67%) | 71 (72%) |
| *A*3 | 950 (9%) | 1800 (0%) | 3300 (30%) | 96 (63%) | 188 (30%) | 286 (14%) |
| *D*1 | 700 (33%) | 1050 (42%) | >5000 (>6%) | 178 (32%) | 178 (34%) | 177 (29%) |
| *D*2 | 1040 (0%) | 1400 (22%) | >5000 (>6%) | 356 (37%) | 261 (3%) | 177 (29%) |

## 6. Discussion

The results even for relatively low frequencies indicate that the sampling variant substantially influences the electric drive control dynamics, as expected from [14] and [15]. For the Bode plots, the corner frequency at which the magnitude drops to 3 dB (0.71 p.u.) is similar among all the considered models for $m = 0$, but differences between the results increase with $m$. Analog model *A*3 and digital models *D*1 and *D*2 present the best similarity to the reference across all values of $m$. The maximum phase drop is not represented well (Table 3) by any of the models for all values of $m$. For the frequency characteristics, only digital model *D*2 tracks the reference phase reasonably for most of the frequency range.

For frequencies up to 1000 Hz, digital model *D*2 is closest to the reference in both magnitude and phase. Although this frequency range is sufficient for currently considered vehicle safety systems, it may be surpassed by future needs. In the range of frequencies above

1000 Hz, digital model *D*2 provides the closest phase graph to the reference, but also results from digital model *D*1 and analog model *A*3 are good. Matching magnitude in this frequency range is highly frequency dependent, with analog model *A*1 constantly being clearly the worst.

Analog models *A*1 and *A*2 are unsuitable for the stability analysis of the speed control (outer) loop because their phase characteristics are generally above the characteristics of other models for all values of *m*. Indeed, even after adding a controller for the speed control, the resulting phase characteristics of the speed control will remain shifted up relative to the reference model.

What clearly differentiates the considered models and allows to select the best ones, is their performance in the time domain, not in the frequency domain. Considering the measures obtained for the step response, analog models offer the most precise results in rise time. Analog models *A*2 and *A*3 excel in this regard for all values of *m*, model *A*1 only follows closely the rise time for $m = 1$. Digital models are characterized by substantial inaccuracy in representing rise time, which partially results from their discrete output update, which takes place once per control cycle. In turn, overshoot is modeled well only with the digital models, with *D*2 offering a good approximation for all values of *m*. The settling time for all values of *m* is also better modeled with the digital models. Models *D*1 and *D*2 offer a similar deviation from the reference value, with *D*2 being only slightly better than *D*1.

By overlying the results of time domain analysis on the results of frequency domain analysis, it can be noted that the model *A*3 best reflects the frequency characteristics and the rise time, while the model *D*2 performs correctly in the frequency domain and in the remaining time domain characteristics.

## 7. Conclusion

This paper considers five different analytical models, three analog ones and two digital ones. The frequency and step-response characteristics of the models are compared with those of a reference hybrid model of a real drive, for three different sampling instants within the control cycle. This offers many measures to compare the control dynamics. Depending on the details of the application and the exact requirements regarding control quality, different models are preferable, as described in the previous section.

As expected, generally the level of details included in a model corresponds to the accuracy of the results. Nevertheless, even results from the most sophisticated transfer functions considered do not match the reference for all timing variants and quality measures. For instance, *A*3 provides the best accuracy among the analog models for $m = 0$ and $m = 0.5$, but its time characteristics for $m = 1$ are even worse than those of the simpler models. Hence, selection of the in-wheel drive's modeling approach shall depend on the considered timing scenario and on the criteria of system analysis. The results presented in this paper may support choosing a suitable model for a particular case.

Control system design in the *s*-domain has been widely applied since a long time, and offers many convenient design methods. Despite this advantage, analog models can only be

useful for representing digitally controlled drives if overshoot is not a critical problem for a considered application. However, analog models represent the rise time well, which is a common aim. Digital model *D*2 appears to have the best overall representation of all evaluated parameters for the step response.

It is clear from the simulations that selecting different current sampling instants represented by the value of *m* influences both the time-based and the frequency-based characteristics of the modeled drive system. Thus, future work shall aim to use the *A*3 and *D*2 models to design and analyze the PMSM drive for vehicle traction control applications with different sampling variants.

## References


[1] Bera T.K., Bhattacharya K., Samantaray A.K., *Evaluation of antilock braking system with an integrated model of full vehicle system dynamics*, Simulation Modelling Practice and Theory, no. 19, pp. 2131-2150 (2011).

[2] Cabrera J.A., Castillo J.J., Carabias E., Ortiz A., *Evolutionary Optimization of a Motorcycle Traction Control System Based on Fuzzy Logic*, IEEE Transactions on Fuzzy Systems, vol. 23, no. 5, pp. 1594-1607 (2015).

[3] Ha H., Kim J., Lee J., *Cornering stability enhancement algorithm for in-wheel electric vehicle*, 2014 IEEE International Conference on Industrial Technology (ICIT), pp. 806-809 (2014).

[4] Ivanov V., Savitski D., Shyrokau B., *A Survey of Traction Control and Anti-lock Braking Systems of Full Electric Vehicles with Individually-Controlled Electric Motors*, IEEE Transactions on Vehicular Technology, vol. 64, no. 9, pp. 3878-3896 (2015).

[5] Guo H., Yu R., Qiang W., Chen H., *Optimal slip based traction control for electric vehicles using feedback linearization*, International Conference on Mechatronics and Control, pp. 1159-1164 (2014).

[6] Zhang Z., Zhang J., Sun D., Lv C., *Research on control strategy of electric-hydraulic hybrid anti-lock braking system of an electric passenger car*, 2015 IEEE Intelligent Vehicles Symposium (IV), pp. 419-424 (2015).

[7] Kondratiev I., Nikiforov A., Veselov G., Kolesnikov A., *Synergetic control for induction motor based wheel-drive system*, 2012 IEEE Int. Electric Vehicle Conference (IEVC), pp. 1-7 (2012).

[8] M'sirdi N.K., Rabhi A., Fridman L., Davila J., Delanne Y., *Second Order Sliding-Mode Observer for Estimation of Vehicle Dynamic Parameters*, International Journal of Vehicle Design, vol 48, no. 3/4, pp. 190-207 (2008).

[9] Petersen I., *Wheel Slip Control in ABS Brakes using Gain Scheduled Optimal Control with Constraints*, PhD Thesis, Norwegian University of Science and Technology, Trondheim (2003).

[10] Xiong L., Yu Z.,, *Vehicle Dynamic Control of 4 In-Wheel-Motor Drived Electric Vehicle*, Electric Vehicles - Modelling and Simulations, ed. Seref Soylu, InTech (2011).

[11] Savitski D., Ivanov V., Augsburg K., Shyroka B., Wragge-Morley R., Pütz T., Barber P., *The new paradigm of an anti-lock braking system for a full electric vehicle: experimental investigation and benchmarking*, Proceedings of the Institution of Mechanical Engineers, Part D: Journal of Automobile Engineering, vol. 230, no. 10, pp. 1364-1377 (2015).

[12] Opalinski A., Jarzebowicz L., *Analytical modeling of electric drives for vehicle traction control systems*, 11th Interntional Conference on Ecological Vehicles and Renewable Energies (EVER), Monte-Carlo (2015).

[13] Banks J., Chwif L., *Wornings about simulation*, Journal of Simulation, vol. 279, no. 5 (2011).

[14] Böcker J., Buchholz O., *Can oversampling improve the dynamics of PWM controls?*, IEEE International Conference on Industrial Technology (ICIT), Cape Town, pp. 1818-1824 (2013).

[15] Jarzebowicz L., Opalinski A., Cisek M., *Improving Control Dynamics of PMSM Drive by Estimating Zero-Delay Current Value*, Elektronika ir Elektrotechnika, vol. 21, no. 2, pp. 20-23 (2015).

[16] Anuchin A., Kozachenko V., *Current loop dead-beat control with the digital PI-controller*, 16th European Conference on Power Electronics and Applications (EPE'14-ECCE), pp. 1-8 (2014).
[17] Hinkkanen M., Awan H.A.A., Qu Z., Tuovinen T., Briz F., *Current Control for Synchronous Motor Drives: Direct Discrete-Time Pole-Placement Design*, IEEE Transactions on Industry Applications, vol. 52, no. 2, pp. 1530-1541 (2016).
[18] Vajta M., *Some Remarks on Pade-Approximation*, 3rd TEMPUS-INTCOM Symposium (2000).
[19] Silva G.J., Datta A., Bhattacharyya S.P., *Controller design via Pade approximation can lead to instability*, 40th IEEE Conference on Decision and Control, vol. 5, pp. 4733-4737 (2001).
[20] Time R.J., *Delay Systems: An Overview of Some Recent Advances and Open Problems*, Automatica, vol. 39, pp. 1667-1694 (2003).
[21] Gu D-W., Petkov H.P., Konstantinov M.M., *Robust Control Design with MATLAB*, 2-nd Ed., Springer (2013).
[22] Jury E.I., *Theory and Application of the Z-Transform Method*, R. E. Krieger Publishing Company (1973).
[23] Czerwinski R., Rudnicki T., *Examination of electromagnetic noises and practical operations of a PMSM motor driven by a DSP and controlled by means of field oriented control*, Elektronika ir Elektrotechnika, vol. 20, no. 5, pp. 46-50 (2014).
[24] Jarzebowicz L., Karwowski K., Kulesza W.J., *Sensorless algorithm for sustaining controllability of IPMSM drive in electric vehicle after resolver fault*, Control Engineering Practice, vol. 58, pp. 117-126 (2017).
[25] Jarzebowicz L., *Errors of a Linear Current Approximation in High-Speed PMSM Drives*, IEEE Transactions on Power Electronics, vol. 32, iss. 11, Nov. 2017, pp. 8254-8257 (2017).
[26] Nam K.H., *AC Motor Control and Electric Vehicle Applications*, CRC Press, p. 9 (2010).